


Hypericum Perforatum-Derived Exosomes-Like Nanovesicles: A Novel Natural Photosensitizer for Effective Tumor Photodynamic Therapy

Xiaoyu Ma, Ni Chen, Peiyuan Zeng, Yuqian He, Tao Zhang, Yu Lu, Ziyu Li , Jin Xu, Jingcan You, Youkun Zheng, Liquan Wang, Mao Luo, Jianbo Wu

Basic Medicine Research Innovation Center for Cardiometabolic Diseases, Ministry of Education; Laboratory for Cardiovascular Pharmacology, Department of Pharmacology, School of Pharmacy; Luzhou Municipal Key Laboratory of Thrombosis and Vascular Biology Southwest Medical University, Luzhou, 646000, People's Republic of China

Correspondence: Jianbo Wu, Basic Medicine Research Innovation Center for Cardiometabolic Diseases, Ministry of Education, Southwest Medical University, Luzhou, Sichuan, 646000, People's Republic of China, Tel/Fax +0086-830-3161702, Email jbwucn1996@yahoo.com

Background: Natural photosensitizers hold potential for photodynamic therapy (PDT) but are often limited by poor visible light absorption. Plant-derived exosome-like nanovesicles offer an innovative platform for enhancing photosensitizer performance.

Methods: Hypericum perforatum-derived nanovesicles (HPDENs) were characterized using electron microscopy, dynamic light scattering, and proteomic and miRNA sequencing. High-performance liquid chromatography confirmed hypericin content. PDT efficacy was assessed in vitro and in vivo.

Results: HPDENs exhibited robust photosensitizing properties, generating reactive oxygen species (ROS) through both Type I and Type II pathways upon light activation. In vitro, HPDENs showed light dose-dependent cytotoxicity against human melanoma cells, characterized by elevated ROS production and apoptosis induction. In vivo, HPDEN-mediated PDT significantly suppressed tumor growth and induced extensive tumor necrosis, with no observable toxicity to major organs.

Conclusion: HPDENs represent a novel plant-derived photosensitizer with dual ROS generation pathways and significant therapeutic efficacy, providing a promising platform for enhancing photodynamic therapy.

Keywords: Hypericum perforatum-derived exosomes-like nanovesicles, photosensitizer, photodynamic therapy, reactive oxygen species, apoptosis

Introduction

Photodynamic therapy (PDT) has emerged as a minimally invasive and highly selective treatment for various diseases, particularly cancer. PDT leverages PHOTSENSITIZERS (PSs) that, upon activation by light of a specific wavelength, generate reactive oxygen species (ROS) capable of inducing oxidative damage and cell death.^{1,2} Despite its potential, PDT faces critical challenges. Current photosensitizers often exhibit insufficient ROS generation, limiting their therapeutic efficacy. Additionally, many PSs, such as porfimer sodium (Photofrin), suffer from poor water solubility, low bioavailability, and suboptimal tumor selectivity, necessitating alternative strategies to improve their performance.

Several naturally and commercially derived PSs illustrate the current challenges and advancements in PDT. For instance, methylene blue, a second-generation PS, improves upon first-generation agents but still struggles with hypoxic tumor environments that reduce ROS production.^{3,4} Chlorin e6 (Ce6), another commercially available PS, exhibits enhanced ROS generation and tumor specificity compared to earlier agents. However, its hydrophobicity poses challenges for clinical applications.⁵ Naturally derived compounds, such as hypericin from *Hypericum perforatum* (St. John's wort), have shown promise due to their high singlet oxygen yield upon light activation, though issues like solubility and stability persist. Recent innovations, including the use of nanotechnology and targeted delivery systems, are addressing these limitations by improving PS selectivity and ROS efficiency.

Exosomes, small extracellular vesicles (30–150 nm), have emerged as promising carriers for therapeutic agents, including PSs. Derived from various cell types, including plants, exosomes can transfer bioactive molecules such as proteins, nucleic acids, and lipids.^{6–8} Plant-derived exosomes, or plant exosome-like nanoparticles, are of particular interest due to their unique properties.⁹ Unlike mammalian exosomes, plant-derived exosomes may contain photosynthetic components, such as chlorophyll and oxygen-evolving complexes, which can enhance ROS production even in hypoxic environments.^{10–14} For example, spinach-derived photosynthetic systems encapsulated in lipid nanoparticles have been shown to increase intracellular ATP and NADPH levels under light exposure, demonstrating their potential in biomedical applications.¹⁵

Among naturally derived photosensitizers, *Hypericum perforatum* has been extensively studied for its medicinal properties.¹⁶ Hypericin, a primary bioactive compound of *H. perforatum*, exhibits strong potential as a photosensitizer for photodynamic therapy (PDT); however, its clinical application is limited by poor solubility, high lipophilicity, instability, and costly production.^{17,18} Addressing these limitations, this study introduces *H. perforatum*-derived exosome-like nanovesicles (HPDENs) as a novel photosensitizer for PDT. The findings highlight enhanced therapeutic efficacy and the added capability for image-based monitoring, offering a dual-functional platform for cancer treatment. These results position HPDENs as a promising candidate for advancing more effective and selective PDT approaches.

Materials and Methods

Reagents and Instruments

All reagents utilized in this study were of analytical grade. Singlet Oxygen Sensor Green (SOSG) was sourced from Thermo Fisher Scientific. Hypericin and Dihydrorhodamine 123 (DHR123) were provided by MedChemExpress (MCE). Reactive oxygen species (ROS) indicators, including 9',10'-anthracenediyl-bis(methylene)-dimalonic acid (ABDA) and 2',7'-dichlorodihydrofluorescein diacetate (DCFH-DA), were obtained from Beyotime Biotechnology Co., Ltd. The FITC Annexin V Apoptosis Detection kit was supplied by BD Biosciences, and the TUNEL kit was purchased from Servicebio Technology Co., Ltd.

Particle size measurements were conducted using a Malvern Zetasizer Nano-S90 (Malvern, UK). UV-Vis absorption spectra were recorded with a Shimadzu UV spectrophotometer (Shimadzu, Japan). Fluorescence measurements were taken using an Edinburgh fluorescence spectrometer (Edinburgh Instruments, UK), and high-performance liquid chromatography (HPLC) analyses were performed on an Agilent 1260 system. Transmission electron microscopy (TEM) images were captured using an HT-7700 microscope. Mass spectrometric (MS) data were acquired using a nanoUPLC (nanoElute2) coupled with a timsTOF Pro2 (Bruker) via a nano-electrospray ionization source. Fluorescence imaging was carried out using a Zeiss LSM7 DUO Laser Scanning Confocal Microscope. In vivo small animal imaging was performed using a Tanon ABL X5 system (Shanghai Tanon Technology Co., Ltd.).

Extraction of *Hypericum Perforatum*-Derived Exosome-Like Nanovesicles (HPDENs)

The material of *Hypericum perforatum* was sourced from Sichuan, China, and voucher specimens have been deposited in the Herbarium of Beijing Forestry University (BJFC) for reference. The specimens were identified by Zhixiang Zhang. The dried *Hypericum perforatum* was ground into fine powder and soaked in PBS overnight. The resulting extract was filtered to remove plant debris, followed by three rounds of refrigerated high-speed centrifugation (4°C, 12,000 rpm for 5, 20, and 60 minutes) to discard the sediment. The supernatant was further filtered through a 0.22 µm membrane and concentrated using an ultrafiltration tube. Exosomes were isolated using a qEV column (IZON, Hua Ying Biotechnology Co., Ltd., China), subjected to ultracentrifugation (4°C, 150,000 rcf for 1.5 hours), and finally resuspended in PBS for storage at 4°C in the dark.

Identification of HPDENs

Transmission Electron Microscopy (TEM)

A 10 µL aliquot of HPDENs was deposited onto a copper grid for visualization via TEM at 100 kV.

Protein Concentration Measurement of HPDENs

The protein concentration of HPDENs was determined using the BCA protein assay kit. A working solution was prepared by mixing solutions A and B from the kit in a 50:1 ratio. A volume of 20 µL of HPDENs and 200 µL of the working

solution were added to each well of a 96-well plate, incubated at 37°C for 30 minutes, and the absorbance at 562 nm was measured using a microplate reader.

Particle Size Analysis

HPDEN particle size was assessed using a NanoFCM instrument. A diluted sample of 10 μ L was analyzed for particle size distribution.

Zeta Potential Measurement

The Zeta potential of HPDENs was determined using a Malvern laser particle size analyzer.

UV Absorption

UV absorption spectra of HPDENs were recorded using a UV spectrophotometer with samples placed in a quartz cuvette.

Fluorescence Spectroscopy

Fluorescence intensity of HPDENs was measured across different wavelength ranges using a fluorescence spectrometer. The emission wavelength was set to 710 nm, and fluorescence was detected between 500–650 nm and 550–800 nm, with excitation at 420 nm.

HPLC Quantification of Hypericin in HPDENs

Hypericin content in HPDENs was determined using HPLC. A standard hypericin solution (2.9 μ g/mL) was prepared, and the peak areas of samples were measured to calculate the hypericin concentration.

Proteomic Analysis of HPDENs

HPDENs were exposed to LED light for 30 minutes and analyzed using nanoUPLC coupled with a timsTOF Pro2. Mass spectrometric data were collected using DDA-PaSEF mode, and peptide identification was performed with the PaSER software (Version 2023). Search parameters included UniProt FASTA databases, with Carbamidomethyl [C] as a fixed modification and Oxidation (M) and Acetyl (Protein Nterm) as variable modifications. Peptide identification allowed up to two missed cleavages, with an FDR of 0.01.

miRNA Sequencing

Total RNA from HPDENs was extracted after LED light exposure using a miRNeasy mini kit. The miRNA sequences were analyzed and mapped against species-specific precursors using BLAST and miRBase 22.1. Differential expression was assessed by ANOVA, and computational tools (GStar, v1.0) were used to predict target genes and annotate GO terms and KEGG pathways.

ROS Detection

General ROS Detection

PBS, HPDENs, and hypericin (10 μ M DCFH-DA) were exposed to LED light at 590 nm (44 mW/cm²) for varying durations (1, 2, 4, 6, 8, 10, 15, and 20 minutes), and fluorescence was measured.

Superoxide Radical Detection

Superoxide anion radicals were detected in a mixture containing PBS, HPDENs, and hypericin (10 μ M DHR123) following LED light exposure at 590 nm (44 mW/cm²) for varying durations (1, 2, 4, 6, 8, 10, 15, and 20 minutes).

Hydroxyl Radical Detection

Hydroxyl radicals were similarly detected using DHR123 after LED light exposure at 590 nm (44 mW/cm²) for varying durations (1, 2, 4, 6, 8, 10, 15, and 20 minutes).

Singlet Oxygen Detection

Singlet oxygen was detected using SOSG in a mixture of PBS, HPDENs, and hypericin after LED light exposure at 590 nm (44 mW/cm²) for varying durations (1, 2, 4, 6, 8, 10, 15, and 20 minutes).

Cell Culture and Assays

WM-266-4 cells were purchased from Hunan Fenghui Biotechnology Co., Ltd., China, and cultured in DMEM supplemented with 10% FBS. For the cellular uptake assay, HPDENs (10 $\mu\text{g/mL}$) were incubated with the cells, followed by DAPI staining for fluorescence microscopy observation. Cell viability was tested using the CCK-8 assay, and ROS levels were measured using DCFH-DA fluorescence detection after LED light exposure at 590 nm (44 mW/cm^2) for 10 minutes.

Immunoblotting

Proteins from WM-266-4 cells were analyzed by immunoblotting using antibodies against BAX, caspase 3, and β -actin.

In vivo Tumor Model

Male BALB/c-nude mice were injected with WM-266-4 cells to induce tumor formation. In vivo fluorescence imaging was conducted following HPDEN injection, and photodynamic therapy was applied using LED light. PDT was administered every three days. One hour after tail vein injection of the drug, the tumor site was irradiated with LED light (590 nm, 70 mW/cm^2) for 10 minutes. The PDT treatment regimen was completed on the 15th day. Tumor growth, body weight, and liver and kidney function were monitored. TUNEL and HE staining were performed on tissue sections for further analysis.

Statistical Analysis

Statistical analyses were conducted using SPSS 24.0, with data presented as mean \pm SEM. Significance between groups was determined using one-way or two-way ANOVA, with $P < 0.05$ considered significant.

Results and Discussion

Characteristics of Hypericum Perforatum-Derived Exosomes-Like Nanovesicles (HPDENs)

Exosomes-like nanovesicles derived from the natural plant *Hypericum perforatum* were obtained through the Size Exclusion Chromatography (SEC) and ultra-high-speed centrifugation methods. The characterization of HPDENs was conducted based on results obtained from transmission electron microscopy images, particle size distribution, and ZETA potential analysis (Figure 1A–C). The illuminated (510–670 nm LED light, 30 mins) and non-illuminated HPDENs exhibited a double-layer cup-and-plate structure (Figure 1A), with an average particle size of approximately 67 ± 3.13 nm (Figure 1B), and the zeta potential was -16.4 ± 0.28 mV (Figure 1C). An exhaustive proteomic analysis was undertaken on both light-treated and non-light-treated HPDENs. The investigation yielded a total of 61 differentially expressed proteins, comprising 25 up-regulated and down-regulated proteins, resulting in 36 distinct species (Supplementary Figure 1A–C). We conducted a miRNA sequencing analysis of HPDENs (Supplementary Figure 1D–F), which indicated differential expression of 82 types of miRNA following exposure to light, with 11 types up-regulated and 71 types down-regulated.

The physical and chemical properties of these exosomes were further examined using a UV-visible spectrophotometer and a fluorescence spectrophotometer (Figure 1D–F). UV-visible spectrophotometry results indicated that HPDENs exhibited maximum absorption at 598 nm (Figure 1D). Additionally, the fluorescence spectrophotometer revealed that HPDENs were self-fluorescent and demonstrated fluorescence properties in polar solvents such as PBS, suggesting the potential for these exosomes to serve as a natural imaging agent (Figure 1E and F). The prepared HPDENs were subjected to stability tests by storing them at 4°C in a lightproof environment for 7 days. The relative size distribution ($S/S_0 \times 100\%$) (Figure 1G) and UV-Vis absorption intensity ($A/A_0 \times 100\%$) (Figure 1H) were measured and remained consistent throughout the testing period. However, the relative fluorescence intensity ($F/F_0 \times 100\%$) showed a slight decrease over time (Figure 1I).

To delve deeper into the composition of HPDENs, high-performance liquid chromatography (HPLC) analysis was employed (Figure 1J). The chromatographic results demonstrated identical retention times for both HPDENs and hypericin, providing compelling evidence for the presence of hypericin within the HPDENs. The quantification of hypericin within the HPDENs relative to a hypericin standard was achieved through the external standard method, yielding a ratio of 1:97.05 (1.03%) (Figure 1K). This meticulous analysis confirms the encapsulation of hypericin within the HPDENs, shedding light on their potential applications in targeted drug delivery and imaging modalities.

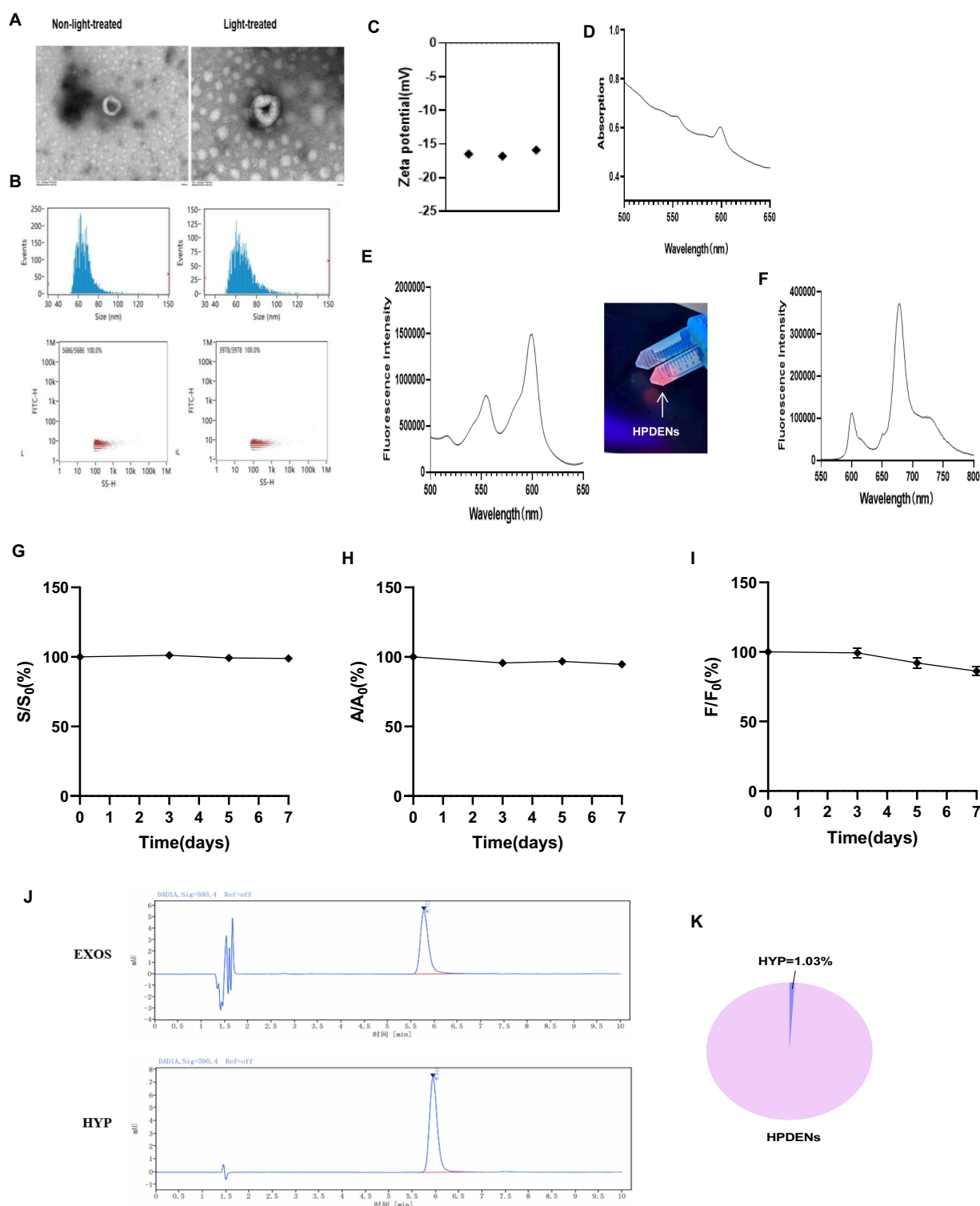


Figure 1 Characteristics of HPDENs. **(A)** Transmission electron microscopy (TEM) images depicting HPDENs with and without illumination. Scale bar: 100 nm. **(B)** Particle size distribution of HPDENs, as determined by dynamic light scattering. **(C)** Measurement of HPDENs surface potential utilizing a Malvern laser particle sizer: (n=3) **(D)** UV-visible spectrophotometry used to assess the UV absorption of exosomes. **(E)** Fluorescence spectrophotometry measuring the excitation light spectrum of HPDENs. Excitation wavelength (Ex): 710 nm, Emission wavelength (Em): 500–650 nm. **(F)** Fluorescence spectrophotometry assessing the emission light spectrum of exosomes. Excitation wavelength (Ex): 420 nm, Emission wavelength (Em): 550–800 nm. Stability testing of HPDENs was conducted at 4°C in a lightproof environment for 7 days. Throughout the testing period, the relative size distribution ($S/S_0 \times 100\%$) **(G)**, UV-Vis absorption intensity ($A/A_0 \times 100\%$) **(H)**, and fluorescence intensity ($F/F_0 \times 100\%$) **(I)** were measured. Data were collected from triplicate measurements and presented as means \pm SEM. S represents size; A represents absorbance; F represents fluorescence. **(J and K)** High-performance liquid chromatography (HPLC) analysis of HPDENs compared with a hypericin standard. Peak area was calculated using the external standard method.

HPDENs Exhibit Photosensitizer Properties

To investigate the potential of HPDENs as natural photosensitizers, we conducted separate analyses on singlet oxygen ($^1\text{O}_2$), superoxide anion radical ($\cdot\text{O}_2^-$), hydroxyl radical ($\cdot\text{OH}$), and total reactive oxygen species (ROS) generation (Figure 2A–D). Singlet oxygen production was assessed using SOSG, a specific probe that emits green fluorescence upon reacting with singlet oxygen. The experiment comprised three groups: PBS as the control, the hypericin (HYP) group as the positive control, and the HPDENs as the experimental group. Upon irradiation with a 590 nm wavelength LED light at an optical power of 44mW/cm² and subsequent fluorescence detection using a spectrophotometer, our results demonstrated a substantial increase in singlet oxygen

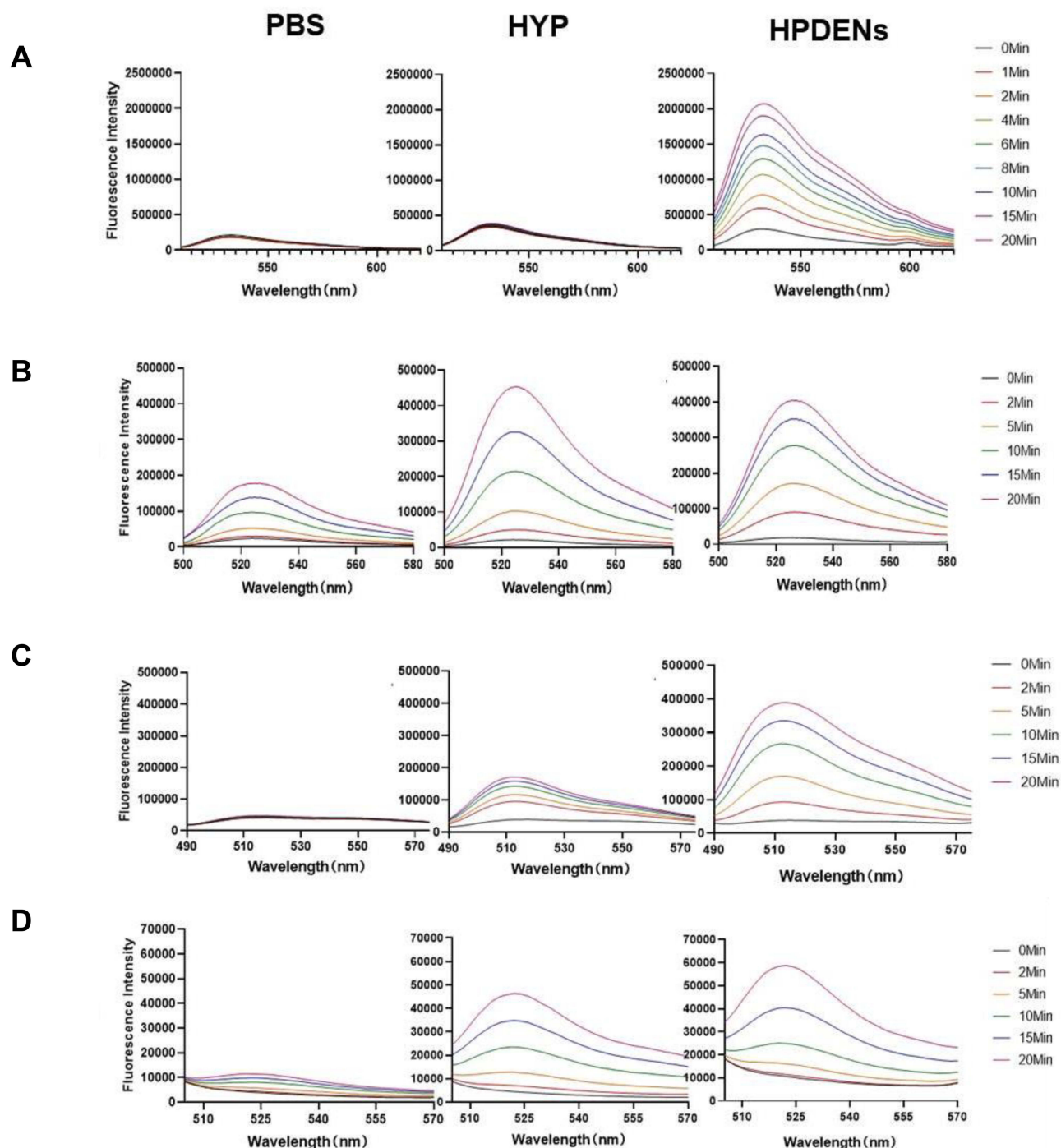


Figure 2 Continued.

E

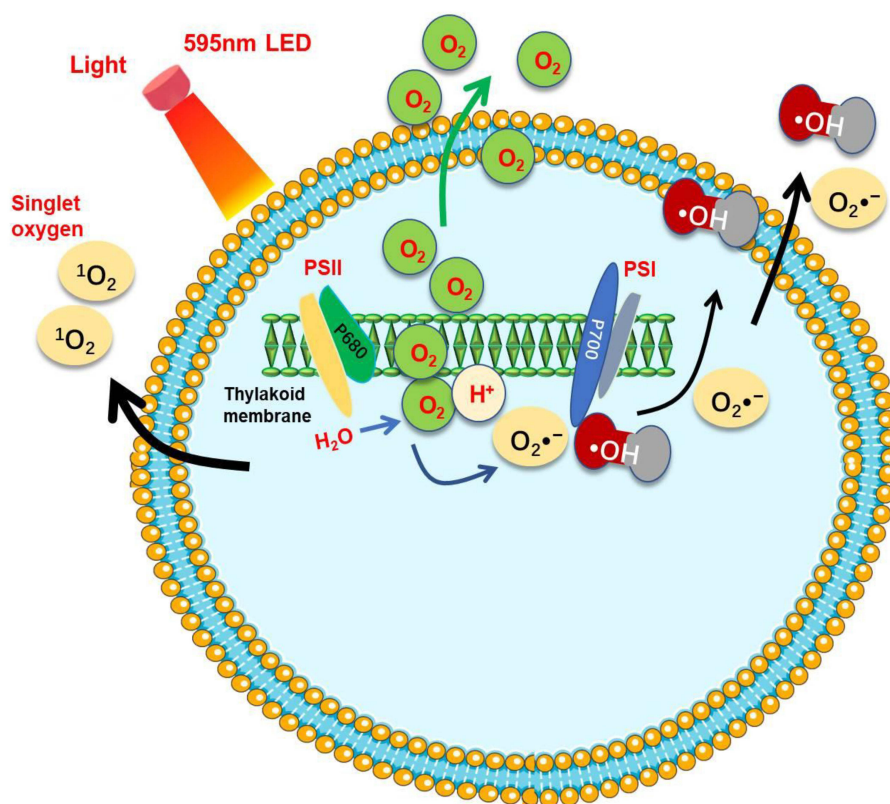


Figure 2 HPDENs exhibit photosensitizer properties. **(A)** Singlet oxygen ($^1\text{O}_2$) measurement was conducted using a fluorescence spectrophotometer to detect fluorescence intensity at 0, 1, 2, 4, 6, 8, 10, 15, and 20 minutes of illumination, with excitation at 504 nm and emission range of 510–620 nm. **(B)** Superoxide anion radical ($\text{O}_2^{\bullet-}$) measurement was performed using a fluorescence spectrophotometer to detect fluorescence intensity at 0, 2, 5, 10, 15, and 20 minutes after illumination, with excitation at 480 nm and emission range of 550–580 nm. **(C)** Hydroxyl radical ($\cdot\text{OH}$) measurement utilized a fluorescence spectrophotometer to detect fluorescence intensity at 0, 2, 5, 10, 15, and 20 minutes after illumination, with excitation at 480 nm and emission range of 490–575 nm. **(D)** Total reactive oxygen species (ROS) were assessed using a fluorescence spectrophotometer to detect fluorescence intensity at 0, 2, 5, 10, 15, and 20 minutes after illumination, with excitation at 480 nm and emission range of 505–570 nm. **(E)** Schematic illustration of HPDENs exhibiting characteristics of both Type I and Type II photosensitizers.

production from HPDENs with prolonged illumination time, which was 69.98 times higher than HYP group. In contrast, minimal singlet oxygen was detected in both the PBS and HYP groups, indicating that HPDENs function as a type II photosensitizer (Figure 2A). HPDENs demonstrated a substantial increase in singlet oxygen production with prolonged illumination time.

Subsequently, we investigated the generation of superoxide anions post-photoactivation. Dihydrorhodamine 123 (DHR123) was employed as a specific probe for superoxide anion radicals. It undergoes conversion to rhodamine 123 in the presence of superoxide anion radicals, emitting green fluorescence. The experiment involved PBS, HYP, and HPDENs groups. Increasing illumination time resulted in a rise in fluorescence intensity in both the HYP and HPDENs groups (Figure 2B). Furthermore, we examined the generation of hydroxyl radicals using hydroxyphenylfluorescein (HPF) as the probe. Our results revealed that as the illumination time increased, the HPDENs and HYP groups produced highly cytotoxic hydroxyl radicals, with the HPDENs group showing 2.75 times higher hydroxyl radical production compared to the HYP group (Figure 2C). Finally, we explored the production of total ROS using the probe DCFH-DA. The findings demonstrated that as the illumination time increased, both the HYP and HPDENs groups produced reactive oxygen species. After 20 minutes of illumination, the total ROS production in the HPDENs group was 1.18 times higher than that in the HYP group (Figure 2D). Our experimental results suggest that HPDENs exhibit characteristics of both Type I and Type II photosensitizers (Figure 2E).

Photodynamic Effects of HPDENs on Tumor Cells

We proceeded with an investigation into the inhibitory effects of photodynamic HPDENs on human melanoma cells, WM-266-4 cells in vitro. Initially, we conducted exosome uptake experiments to validate the internalization of HPDENs, which were distinguished by red fluorescence markers. The fluorescence intensity exhibited a progressive increase from 0

to 12 hours, reaching its peak at the 12-hour mark and remaining stable until the 24-hour time point with only minimal attenuation. This observation strongly suggests the successful uptake of HPDENs by the cells following co-culture, establishing a significant treatment time frame within the cells (Figure 3A and B). We examined the influence of

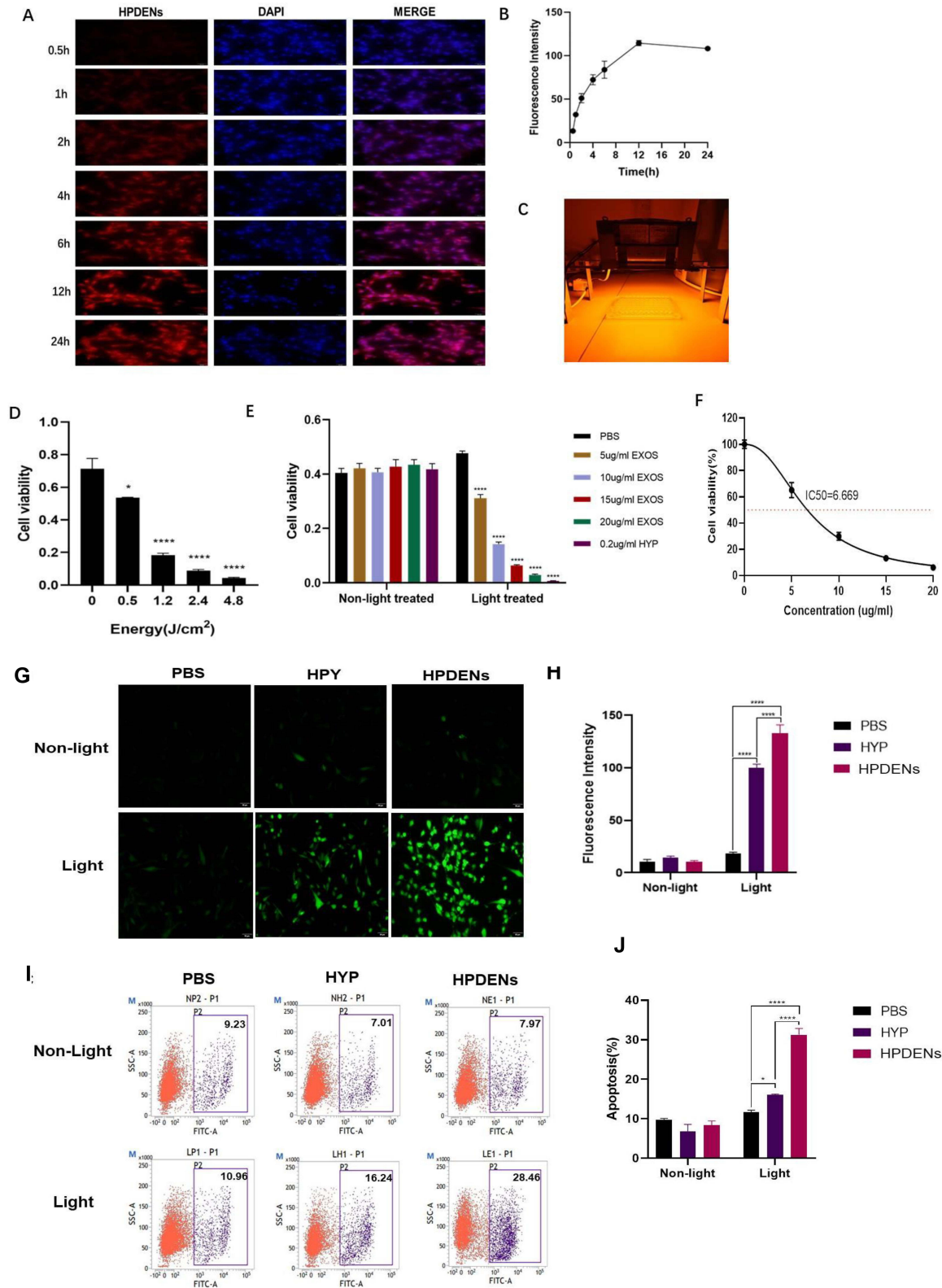


Figure 3 Continued.

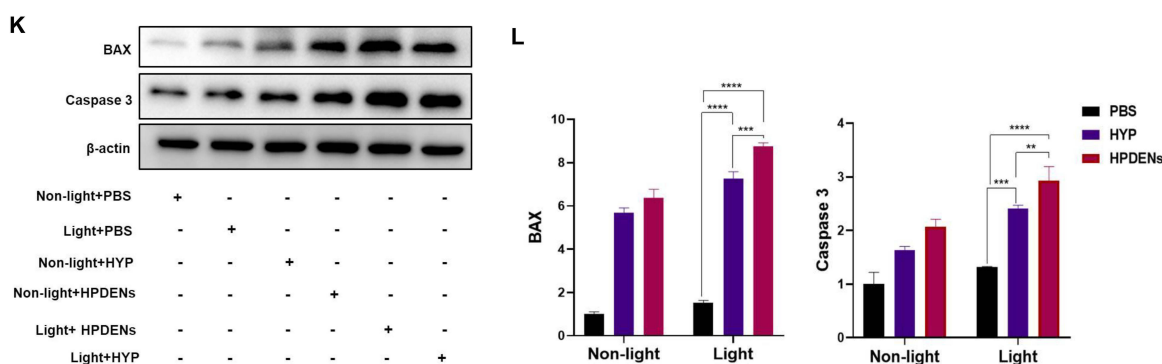


Figure 3 Photodynamic effects of HPDENs on tumor cells. **(A)** Fluorescence microscopy image illustrating the uptake of HPDENs in WM-266-4 cells. Scale bar: 50 μ m. **(B)** Changes in fluorescence intensity over time after melanoma cells internalized HPDENs. $n=3$. **(C)** WM-266-4 cells were illuminated with an LED emitting light at a wavelength of 590 nm and an intensity of 4 mW/cm². **(D)** WM-266-4 cells were treated with HPDENs for 12 hours were subjected to varying LED irradiation energies to assess cell viability. Data are expressed as means \pm SEM. **(E)** WM-266-4 cells were co-cultured with different concentrations of HPDENs for 12 hours. The PBS group served as the negative control, while the HYP group served as the positive control. Cells were then irradiated with an LED at 4 mW/cm² for 10 minutes or left untreated. Data are expressed as means \pm SEM. **(F)** The IC₅₀, representing the inhibitory concentration at which 50% of cell viability was reduced, was calculated based on the effect of various concentrations of HPDENs on WM-266-4 cells viability under LED irradiation. **(G)** Fluorescence microscopy images depict cellular reactive oxygen species levels following treatment with PBS, HYP, and HPDENs with or without LED illumination. Scale bar: 100 μ m. **(H)** Graphic represents cellular ROS levels observed in fluorescence microscopy images. $n=3$. Data are expressed as means \pm SEM. **(I and J)** Flow cytometry was employed to assess the expression of apoptosis-related genes in Annexin V-labeled cells. Quantitation of FITC-positive results obtained through flow cytometry. $n=3$. Data are expressed as means \pm SEM. **(K and L)** Representative immunoblots of BAX and caspase 3 from WM-266-4 cells as indicated. All graphs correspond to the adjacent blots above and represent densitometric analyses of 3 independent experiments. P-values indicating the significance of difference are indicated in the respective bar diagrams. All group data are shown as mean \pm SEM. * $p < 0.05$; ** $p < 0.05$; *** $p < 0.001$; **** $p < 0.0001$.

photodynamic HPDENs on cell viability. After a 12-hour co-culture of exosomes with cells, we exposed the cells to irradiation using a 590 nm, 4mW/cm² LED light at various energy intensities (Figure 3C). The findings revealed a progressive decline in cell viability as the light energy increased (Figure 3D).

Furthermore, we conducted co-cultures of cells with HPDENs at various concentrations for 12 hours. The hypericin (HYP) group was used as a positive control, followed by cell irradiation with a light intensity of 4mW/cm² for 10 minutes. Our results revealed a decrease in cell viability in the light-exposed group as the exosome concentration increased. Conversely, the cell viability in the non-irradiated group showed no significant change. This indicates that following photodynamic therapy, HPDENs effectively suppress the growth activity of melanoma cells in a concentration-dependent manner, with an IC₅₀ value of 6.669 μ g/mL (Figure 3E and F).

We started analyzing the production of ROS and apoptosis of WM-266-4 cells. Cells were treated with 10 μ g/mL of HPDENs for 12 hours, divided into two groups for the study: light and non-light conditions. Our results showed no significant increase in ROS levels in the non-light and light PBS groups. However, the light treated HYP group and HPDENs group exhibited a marked increase in ROS levels (Figure 3G). Notably, the fluorescence intensity of the HPDENs group was 1.42 times higher than that of the HYP group, consistent with prior findings where total ROS in the HPDENs group was 1.36 times higher than in the HYP group (Figure 3H). Following this, we investigated the impact of HPDENs on melanoma cell apoptosis post-photodynamic therapy. Flow cytometry results indicated a significant increase in Annexin V expression in both the HYP and HPDENs groups after photodynamic treatment, highlighting a notable induction of cell apoptosis. In contrast, there was no observable change in the PBS group (Figure 3I and J). The Western blot results revealed a significant increase in the expression of Caspase 3 and Bax in WM-266-4 cells of the HPDENs +Light group compared to the other groups (Figure 3K and L). These findings provide confirmation that the combination of HPDENs and PDT leads to a substantial elevation in ROS levels within tumor cells, consequently inducing apoptosis.

In vivo PDT of HPDENs

To elucidate the in vivo anti-tumor potential of HPDENs, we established tumors in nude mice with an initial volume of approximately 100 mm³. Mice were then intravenously administered PBS, HYP (0.25 mg/kg), and HPDENs (1 mg/kg) and subsequently divided into light and non-light treatment groups for photodynamic therapy. As illustrated in Supplementary Figure 2, the temperature of tumors remained relatively constant (36.0–37.9°C) during a 10-minute irradiation. Treatment

was continued until the 15th day, during which we meticulously recorded the body weight and tumor size of the nude mice. The biodistribution of HPDENs was assessed, demonstrating the efficient homing and accumulation of HPDENs at the tumor site within 12 hours post-injection via the tail vein (Supplementary Figure 3A–D). After 15 days of photodynamic therapy, visible tumor necrosis was observed in the light-treated HYP and HPDENs groups, while no significant changes were seen in the non-light-treated and light-treated PBS groups (Figure 4A). Body weight remained stable throughout the 15-day period (Figure 4B). Notably, tumor tissue growth in the light-treated HYP and HPDENs groups was markedly suppressed, presenting significantly smaller volumes compared to the non-light-treated group and the light-exposed PBS group (Figure 4C and D). HE staining revealed minimal necrosis in the non-illuminated and illuminated PBS groups, with tumor cells arranged in nests. In contrast, the illuminated HYP and HPDENs groups exhibited distinct necrotic areas (Figure 4E). TUNEL staining demonstrated increased apoptotic tumor cells in the light-treated HYP and HPDENs groups, which was lower in the non-illuminated and PBS groups (Figure 4F and G). These findings underscore the potent anti-tumor efficacy of HPDENs in vivo.

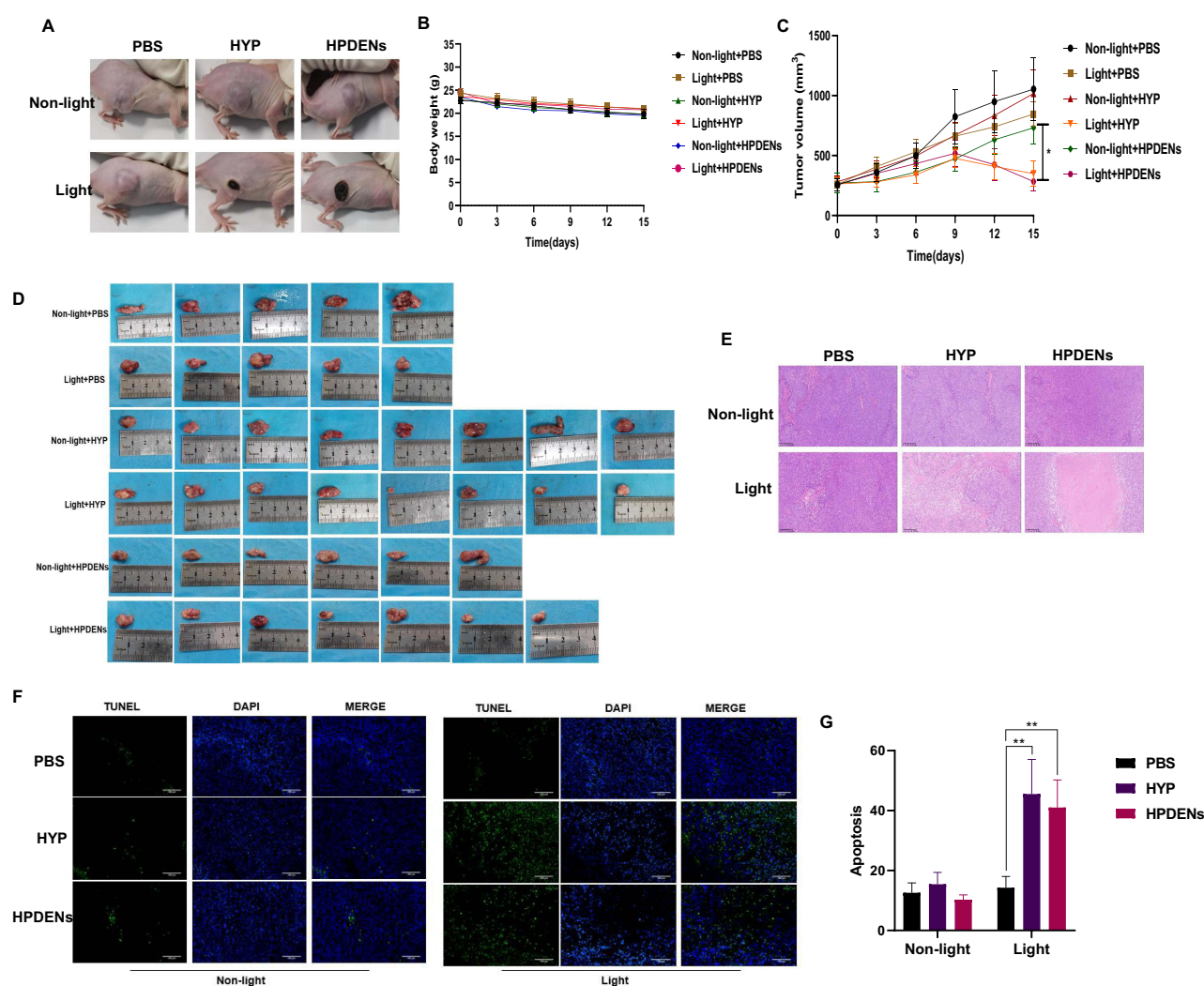


Figure 4 Anti-tumor effect of HPDENs in vivo PDT. (A) Tumor appearance after 15 days of photodynamic therapy in WM-266-4 cells tumor-bearing nude mice. (B) Body weight changes of nude mice during 15 days of photodynamic therapy. $n=5-8/\text{group}$. (C) Tumor volume changes during 15 days of photodynamic therapy. $n=4-8/\text{group}$. $*p < 0.05$. (D) Anatomical image of tumor volume size after 15 days of photodynamic therapy. $n=5-8/\text{group}$. (E) HE staining image of tumor tissue sections 15 days after photodynamic therapy. Arrows show areas of necrosis. (F) Microscopic image of TUNEL fluorescence staining of tumor tissue in nude mice with tumors after 15 days of photodynamic therapy. Scale bar, 100 μm . (G) Quantitation of FITC-positive results obtained in TUNEL fluorescence staining of tumor tissue. $n=3/\text{group}$, $**p < 0.01$. Data are means \pm SEM.

Biocompatibility of HPDENs

To assess the biocompatibility of HPDENs post-PDT in vivo, we performed Hematoxylin and Eosin (HE) staining and sectioning of the hearts, livers, spleens, lungs, and kidneys of nude mice injected with PBS and HPDENs. The results exhibited no discernible damage in the major organs of mice injected with either PBS or HPDENs (Figure 5A). Subsequent serum analysis was conducted to evaluate liver and kidney function, revealing no significant differences between the HPDENs and PBS groups, as all liver and kidney function biomarkers fell within normal ranges (Figure 5B). These findings indicate that the injection of HPDENs into nude mice does not result in observable organ damage or liver and kidney toxicity, thereby suggesting favorable biocompatibility of HPDENs.

We present a multifunctional novel plant-derived photosensitizer, HPDENs derived from *Hypericum perforatum*, as identified photodynamic properties with a fluorescent image. HPDENs exhibit dual Type I and II photosensitizer properties, robustly generating reactive oxygen species (ROS) that significantly reduce melanoma cell viability and promote increased apoptosis in vitro. In vivo studies further demonstrate the efficacy of HPDENs in targeting and suppressing tumor growth without inducing organ toxicity (Figure 6). These findings warrant further exploration of HPDENs for potential applications in targeted drug delivery and PDT modalities.

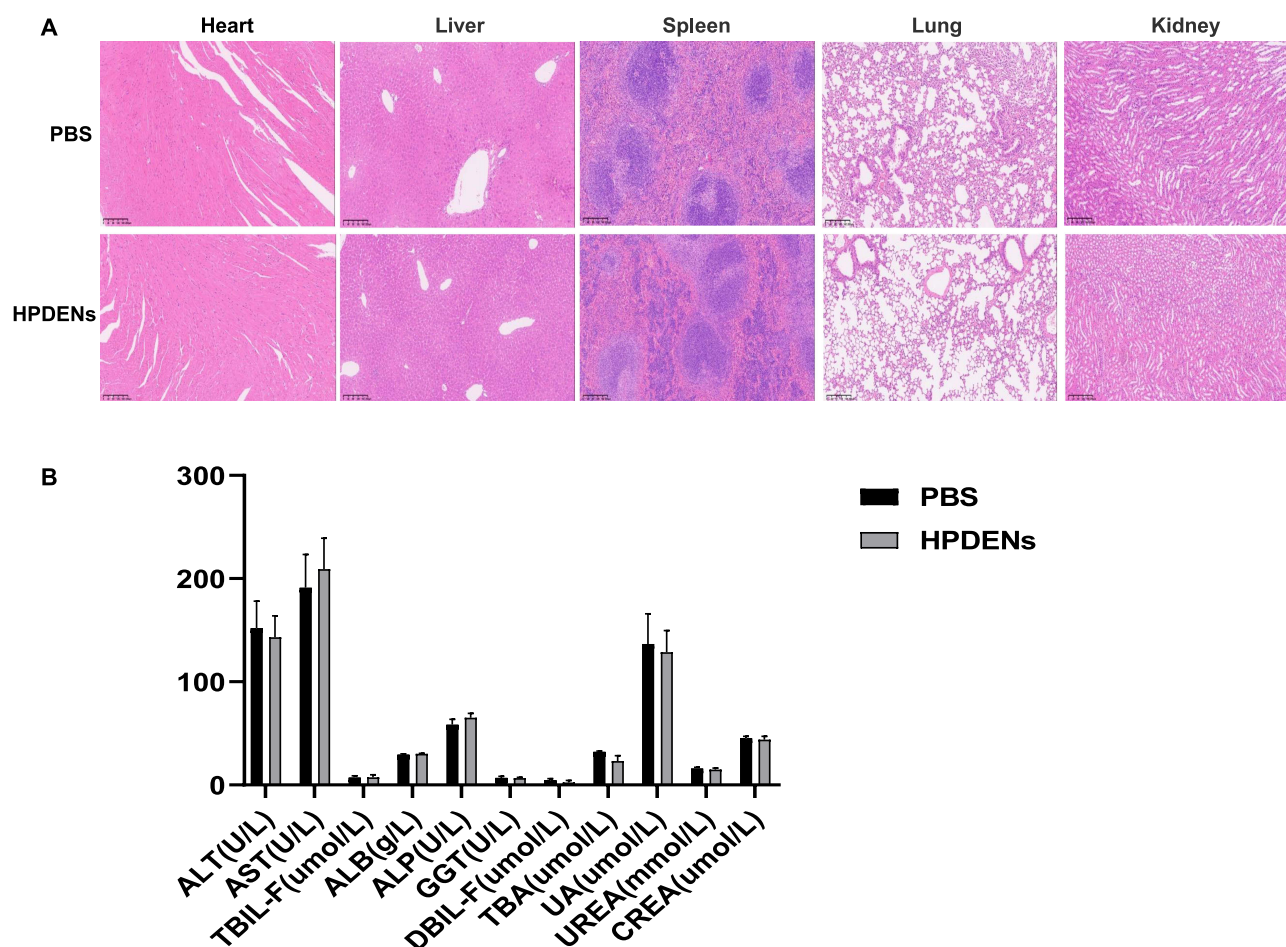


Figure 5 Biocompatibility of HPDENs. (A) Hematoxylin and eosin (HE) stained sections of major organs (heart, liver, spleen, lung, kidney) from nude mice injected with either PBS or HPDENs via the tail vein. Scale bar: 100 μ m. (B) Biochemical indicators of liver and kidney function in nude mice injected with either PBS or HPDENs via the tail vein. Each group comprised n=3 mice. Data are presented as means \pm SEM.

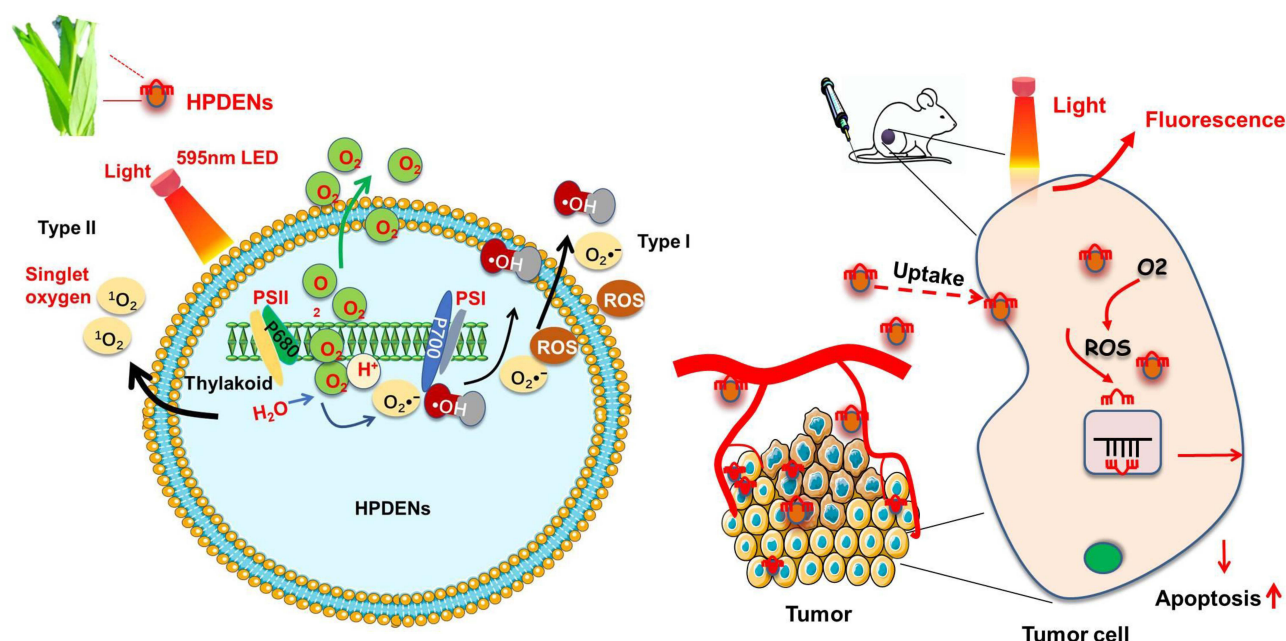


Figure 6 Schematic diagram of HPDENs in tumor PDT process. The schematic diagram illustrates the role of HPDENs as dual-functional agents in tumor PDT. Following targeted delivery to the tumor site, HPDENs generate reactive oxygen species (ROS) upon light activation, inducing apoptosis in tumor cells. Their inherent fluorescence enables real-time imaging for monitoring treatment efficacy. In vivo studies confirm that HPDENs effectively suppress tumor growth with minimal toxicity to healthy tissues, underscoring their potential for safe and targeted clinical applications in PDT.

Conclusion

This study presents *Hypericum perforatum*-derived exosome-like nanovesicles (HPDENs) as a novel photosensitizer for photodynamic therapy (PDT), demonstrating enhanced reactive oxygen species (ROS) production and addressing key limitations of free hypericin, such as poor solubility, bioavailability, and tumor selectivity. HPDENs offer improved stability, targeted delivery, and biocompatibility, distinguishing them from traditional hypericin-based therapies. However, further investigation into their interactions with the tumor microenvironment, including immune and stromal cells, is essential to fully elucidate their mechanism of action and optimize their clinical applicability in PDT.

Abbreviations

ABDA, 9',10'-anthracenediyl-bis(methylene)-dimalonic acid; DCFH-DA, 2',7'-dichlorodihydrofluorescein diacetate; DHR123, Dihydrorhodamine 123; HPDENs, *Hypericum perforatum*-derived exosomes-like nanovesicles; HPLC, high-performance liquid chromatography; LED, Light Emitting Diode; O_2 , superoxide anion radical; 1O_2 , singlet oxygen; OH, hydroxyl radical; PDT, photodynamic therapy; ROS, reactive oxygen species; SOSG, singlet oxygen sensor green; TEM, Transmission Electron Microscopy.

Ethics Approval and Consent to Participate

All animal experiments received approval from the Animal Ethics Committee of Southwest Medical University in accordance with Institutional Animal Care and Use Committee guidelines (Project identification code: NO.20211117-019).

Author Contributions

All authors made a significant contribution to the work reported, whether that is in the conception, study design, execution, acquisition of data, analysis and interpretation, or in all these areas; took part in drafting, revising or critically reviewing the article; gave final approval of the version to be published; have agreed on the journal to which the article has been submitted; and agree to be accountable for all aspects of the work.

Funding

This work was supported by the National Natural Science Foundation of China Grant (81570263, 82370419, and 81970260), Sichuan Province Science and Technology Agency Grant (2024NSFSC0591), and Luzhou-Southwest Medical University Cooperation Project (23YKDCXY0003).

Disclosure

The authors declare that there is no conflict of interest regarding the publication of this paper.

References

- Allison RR, Mota HC, Bagnato VS, Sibata CH. Bio-nanotechnology and photodynamic therapy—state of the art review. *Photodiagnosis Photodyn Ther*. 2008;5(1):19–28. doi:10.1016/j.pdpdt.2008.02.001
- Li X, Lovell JF, Yoon J, Chen X. Clinical development and potential of photothermal and photodynamic therapies for cancer. *Nat Rev Clin Oncol*. 2020;17(11):657–674. doi:10.1038/s41571-020-0410-2
- Wu PT, Lin CL, Lin CW, Chang NC, Tsai WB, Yu J. Methylene-blue-encapsulated liposomes as photodynamic therapy nano agents for breast cancer cells. *Nanomaterials*. 2018;9(1):14. doi:10.3390/nano9010014
- Zou MZ, Liu WL, Chen HS, et al. Advances in nanomaterials for treatment of hypoxic tumor. *Natl Sci Rev*. 2020;8(2):nwaa160. doi:10.1093/nsr/nwaa160
- Hak A, Ali MS, Sankaranarayanan SA, Shinde VR, Rengan AK. Chlorin e6: a promising photosensitizer in photo-based cancer nanomedicine. *ACS Appl Bio Mater*. 2023;6(2):349–364. doi:10.1021/acsabm.2c00891
- Regente M, Pinedo M, San Clemente H, Balliau T, Jamet E, de la Canal L. Plant extracellular vesicles are incorporated by a fungal pathogen and inhibit its growth. *J Exp Bot*. 2017;68(20):5485–5495. doi:10.1093/jxb/erx355
- Funk JL, Frye JB, Oyarzo JN, Chen J, Zhang H, Timmermann BN. Anti-Inflammatory effects of the essential oils of ginger (*Zingiber officinale* Roscoe) in experimental rheumatoid arthritis. *PharmaNutrition*. 2016;4(3):123–131. doi:10.1016/j.phanu.2016.02.004
- Ambrosone A, Barbulova A, Cappetta E, et al. Plant extracellular vesicles: current landscape and future directions. *Plants*. 2023;12(24):4141. doi:10.3390/plants12244141
- Yáñez-Mó M, Siljander PR, Andreu Z, et al. Biological properties of extracellular vesicles and their physiological functions. *J Extracell Vesicles*. 2015;4:27066. doi:10.3402/jev.v4.27066
- Dad HA, Gu TW, Zhu AQ, Huang LQ, Peng LH. Plant exosome-like nanovesicles: emerging therapeutics and drug delivery nanoplateforms. *Mol Ther*. 2021;29(1):13–31. doi:10.1016/j.ymthe.2020.11.030
- Woith E, Guerriero G, Hausman JF, et al. Plant extracellular vesicles and nanovesicles: focus on secondary metabolites, proteins and lipids with perspectives on their potential and sources. *Int J mol Sci*. 2021;22(7):3719. doi:10.3390/ijms22073719
- Usui K, Yamamoto H, Oi T, Taniguchi M, Mori H, Fujita Y. Extracellular vesicle-mediated secretion of protochlorophyllide in the cyanobacterium *Leptolyngbya boryana*. *Plants*. 2022;11(7):910. doi:10.3390/plants11070910
- Fitzpatrick D, Aro EM, Tiwari A. True oxygen reduction capacity during photosynthetic electron transfer in thylakoids and intact leaves. *Plant Physiol*. 2022;189(1):112–128. doi:10.1093/plphys/kiac058
- Kusuzaki K, Matsubara T, Murata H, et al. Natural extracellular nanovesicles and photodynamic molecules: is there a future for drug delivery? *J Enzyme Inhib Med Chem*. 2017;32(1):908–916. doi:10.1080/14756366.2017.1335310
- Chen P, Liu X, Gu C, et al. A plant-derived natural photosynthetic system for improving cell anabolism. *Nature*. 2022;612(7940):546–554.
- Chen S, Liu X, Peng C, et al. The phytochemical hyperforin triggers thermogenesis in adipose tissue via a Dlat-AMPK signaling axis to curb obesity. *Cell Metab*. 2021;33(3):565–580.e7. doi:10.1016/j.cmet.2021.02.007
- Russo E, Scicchitano F, Whalley BJ, et al. Hypericum perforatum: pharmacokinetic, mechanism of action, tolerability, and clinical drug-drug interactions. *Phytother Res*. 2014;28(5):643–655. doi:10.1002/ptr.5050
- Skalkos D, Gioti E, Stalikas CD, Meyer H, Papazoglou TG, Filippidis G. Photophysical properties of Hypericum perforatum L. extracts—novel photosensitizers for PDT. *J Photochem Photobiol B*. 2006;82(2):146–151. doi:10.1016/j.jphotobiol.2005.11.001

International Journal of Nanomedicine

Publish your work in this journal

The International Journal of Nanomedicine is an international, peer-reviewed journal focusing on the application of nanotechnology in diagnostics, therapeutics, and drug delivery systems throughout the biomedical field. This journal is indexed on PubMed Central, MedLine, CAS, SciSearch®, Current Contents®/Clinical Medicine, Journal Citation Reports/Science Edition, EMBase, Scopus and the Elsevier Bibliographic databases. The manuscript management system is completely online and includes a very quick and fair peer-review system, which is all easy to use. Visit <http://www.dovepress.com/testimonials.php> to read real quotes from published authors.

Submit your manuscript here: <https://www.dovepress.com/international-journal-of-nanomedicine-journal>

Dovepress
Taylor & Francis Group